Dispersion and purification of $Mo_6S_3I_6$ nanowires in organic solvents

Denis N. McCarthy and Valeria Nicolosi
School of Physics, University of Dublin, Trinity College, Dublin 2, Ireland

Damjan Vengust
Mo6, Teslova 30, 1000 Ljubljana, Slovenia

Dragan Mihailovic
Jozef Stefan Institute, Jamova 39, 1000 Ljubljana, Slovenia

Giuseppe Compagnini
Department of Chemistry, University of Catania, Viale A. Doria 6, 95125 Catania, Italy

Werner J. Blau and Jonathan N. Coleman[a)]
School of Physics, University of Dublin, Trinity College, Dublin 2, Ireland

(Received 4 September 2006; accepted 28 October 2006; published online 10 January 2007)

Sedimentation measurements have been performed on dispersions of $Mo_6S_3I_6$ nanowires in a range of common solvents. By far the best solvents were *N*,*N*-dimethylformamide (DMF) and acetone. Stable dispersions of purified $Mo_6S_3I_6$ nanowires in DMF, with concentrations as high as 0.06 g l^{-1}, could be produced. Detailed analysis of the sedimentation curves showed that the material consisted of three phases, two insoluble phases and one which could be stably dispersed. We associate the insoluble phases with pseudospherical impurities and insoluble nanowires. The sedimenting nanowires tend to be in the form of large diameter bundles, in contrast to the dispersed phase which consists of nanowires arranged in smaller bundles. The average diameters of the nanowire bundles stably suspended in DMF are 12 ± 14 nm. The measured sedimentation time constants of the insoluble nanowires agree very well with theory allowing us to calculate the solid-fluid interaction parameter, β, to be very close to 10^5 Pa. The material could be purified by controlled sedimentation hence the identification of the various phases was confirmed by x-ray photoelectron spectroscopy and scanning electron microscopy. © *2007 American Institute of Physics*.
[DOI: 10.1063/1.2405322]

INTRODUCTION

Many different inorganic, one-dimensional structures have been produced using a variety of techniques[1,2] for use in applications similar to those mooted for carbon nanotubes.[3,4] Recently, a family of one-dimensional materials has been synthesized with the general formula $Mo_6S_{9-x}I_x$.[5] These nanowires have comparable properties to carbon nanotubes,[6] but have several advantages, such as a simple and scalable synthesis[7] and dispersability of some stoichiometries in common solvents.[8–10] Furthermore, unlike carbon nanotubes, these nanowires exist in a small number of stoichiometries, each of which has identical electronic properties. They are produced in a one-step synthetic process, making them much simpler to produce than the previous molybdenum-chalcogenide nanotubes, such as $MoS_2I_{1/3}$.[11] The stoichiometries synthesized so far are $Mo_6S_3I_6$,[5] $Mo_6S_{4.5}I_{4.5}$,[8] and $Mo_6S_2I_8$, all of which have excellent mechanical and electrical properties. Local density approximation band structure calculations of the $Mo_6S_3I_6$ nanowire predict it to be semimetallic,[12] and Ohmic behavior of this stoichiometry has been observed.[13] The $Mo_6S_2I_8$ stoichiometry has been reported to be metallic,[14] while the $Mo_6S_{4.5}I_{4.5}$ nanowire electronic structure has not yet been reported.

The properties of this family of MoSI nanowires show the prospect of many varied applications. The simplest yet investigated is their use as an alternative lubricating additive for oil,[15] due to their low shear modulus.[6] The production of field emission devices from $Mo_6S_3I_6$ nanowires has been demonstrated to be quite simple and the nanowires have been shown to perform well, with stable field emission currents of over 1 μA observed from an individual bundle.[16] As the electronic properties are identical for each stoichiometry, it is not necessary to achieve single nanowires for many applications. This is a significant advantage for the production of conducting composite materials using these nanowires, where they have been shown to have a very low percolation threshold.[17] The high Young's modulus of these materials could also lead to the mechanical reinforcement of composites. Their low shear modulus would suggest that bundles would not be suitable for this, but reinforcement has been demonstrated, although this may be improved upon with single nanowires. However, for the potential of these materials to be achieved in this wide range of applications, simple processing methods will need to be developed. Specifically, the dispersion of each stoichiometry in organic solvents will have to be demonstrated. This is an issue that has hampered the development of carbon nanotubes and has only recently been resolved.[18–20]

Previously, the dispersion properties of the $Mo_6S_{4.5}I_{4.5}$

[a)]Electronic mail: colemaj@tcd.ie

 © 2007 American Institute of Physics

Downloaded 01 Jul 2010 to 134.226.1.229. Redistribution subject to AIP license or copyright; see http://jap.aip.org/jap/copyright.jsp

nanowires in various solvents have been studied and the best solvent and maximum dispersability were determined.[8] That work demonstrated that these nanowires can be purified by allowing the impurities to sediment out of solution, leaving a stable dispersion of nanowires.[8] Here, a similar study for the $Mo_6S_3I_6$ material is presented. Although these two materials are structurally quite similar, they have been shown to have very different dispersion properties due to differences in the arrangement of their surface atoms. This will be demonstrated here, where the dispersability of $Mo_6S_3I_6$ in various solvents is shown to be quite different from the results previously reported for $Mo_6S_{4.5}I_{4.5}$.

In this paper, dispersions of $Mo_6S_3I_6$ nanowires in various solvents have been monitored by measuring their optical transmission as a function of time. The transmission is related to the local concentration in the dispersions and allows the sedimentation of insoluble material to be observed. The data are found to fit well to sedimentation theory.[8,21] Fit parameters were used to determine the best solvents for dispersing the $Mo_6S_3I_6$ nanowires and the maximum amount of nanowires dispersible. It was determined that there are two sedimenting phases in the raw material. These could be separated from the dispersed material by controlled sedimentation. By investigation with x-ray photoelectron spectroscopy (XPS), scanning electron microscopy (SEM), and UV-visible-IR spectroscopy, it was discovered that it is mainly the impurities that sediment out first, with some larger $Mo_6S_3I_6$ nanowire bundles sedimenting over a longer time scale. The majority of the material that remains stably dispersed consists of smaller diameter $Mo_6S_3I_6$ nanowire bundles.

EXPERIMENTAL METHODS AND ANALYSIS

The raw $Mo_6S_3I_6$ nanowire material was synthesized directly from the elemental material,[5] in the same way as $Mo_6S_{4.5}I_{4.5}$ and $Mo_6S_2I_8$ nanowires. In principle, the stoichiometry that is produced depends only on the proportions of the initial elemental material used. All the nanowires exist in the form of bundles of individual nanowires, with each nanowire having a diameter of 0.94 nm.[8] The as-produced nanowire material has traces of MoS_2 present as an impurity,[8] as well as unreacted iodine.[5] In order to remove the iodine, the as-produced material was washed repeatedly with acetone, with UV-visible-IR spectroscopy used to monitor the iodine content during washing. Unfortunately, this also resulted in the loss of small quantities of nanowire material. All of the experimental work presented here was carried out using this washed $Mo_6S_3I_6$ nanowire material.

The washed $Mo_6S_3I_6$ material was dispersed in a range of solvents at a concentration of 0.1 g l^{-1} using a high power sonic tip (120 W, 60 kHz) for 16 min and then a sonic bath (50 W) for 2 h. After transferring each of these dispersions to a 1 cm cuvette, the sedimentation of the dispersions was analyzed by monitoring the transmission of laser pulses ($\lambda = 650$ nm, $t = 10$ ms) through the center of the cuvette for up to 750 h. Four lasers were used and the results were averaged and converted to absorbance, A, using the Beer-Lambert law,

$$A = \ln(I_0/I) = \alpha_{\text{eff}} C_{\text{eff}} l, \tag{1}$$

where I/I_0 is the transmittance of the dispersion, α_{eff} is the effective absorption coefficient, C_{eff} is the effective concentration, and l is the path length. We use the subscript "eff" as we actually probe the absorbance of all species in the sample, without knowing the actual absorption coefficient of any phase. As the absorbance is proportional to the effective concentration, it can be scaled to represent C_{eff} by normalizing to the initial concentration (0.1 g l^{-1}).

According to sedimentation theory,[8] the concentration of a nonsoluble component sedimenting out of a liquid is given as a function of time t by

$$C(t) = C_n \exp\left[-\frac{g^2(\rho_s - \rho_l)mb}{f(\beta - p_f)}t\right] = C_n e^{-t/\tau_n}, \tag{2}$$

where C_n is the initial concentration of the species, g is the acceleration due to gravity, ρ_s is the density of the sedimenting phase, ρ_l is the fluid density, m is the mass per sedimentation particle, b is the buoyancy correction factor ($b = 1 - \rho_l/\rho_s$), f is the frictional coefficient given by Stokes' relation, p_f is the fluid pressure, and β is related to the solid-fluid interaction force and has the dimensions of pressure.

Hence a time constant, τ, can be determined for the sedimentation of the system,

$$\tau = \frac{f(\beta - p_f)}{g^2(\rho_s - \rho_l)mb}. \tag{3}$$

We can also modify this model to apply specifically to spherical or cylindrical species. Using Stokes' relations for spherical and cylindrical particles, the time constants can be rewritten as

$$\tau_{\text{spherical}} = \frac{9\eta(\beta - p_f)}{2g^2(\rho_s - \rho_l)^2 a^2}, \tag{4}$$

$$\tau_{\text{cylindrical}} = \frac{6K\eta(\beta - p_f)(3/4)^{1/3}}{g^2(\rho_s - \rho_l)^2(r^2 l)^{2/3}}, \tag{5}$$

where η is the solvent viscosity, a is the spherical radius, K is the drag coefficient, r is the cylindrical radius, and l is the cylinder length.

As there may be many components in the as-produced nanowire materials, there could be many sedimenting phases. In this situation, the total effective concentration measured as a function of time will be

$$C(t) = C_0 + \sum_n C_n e^{-t/\tau_n}, \tag{6}$$

where C_0 is the concentration of the nonsedimenting phase, C_n and τ_n are the initial concentrations and the time constant of the nth sedimenting phase, respectively. Therefore, the total initial concentration, C_{total}, from Eq. (8), is given by

$$C_{\text{total}} = C_0 + \sum_n C_n. \tag{7}$$

As illustrated by Eq. (1), this technique probes the sample absorbance as a function of time. This absorbance is

Downloaded 01 Jul 2010 to 134.226.1.229. Redistribution subject to AIP license or copyright; see http://jap.aip.org/jap/copyright.jsp

the sum of the absorbances for all the species in the sample, some of which may be stable and some of which may be sedimenting.

The absorbance as a function of time $A(t)$ is then

$$A(t) = A_0 + \sum_n A_n e^{-t/\tau_n}, \tag{8}$$

where A_0 is the absorbance due to all the soluble phases,

$$A_0 = \sum_{\text{sol}} \alpha_{\text{sol}} C_{\text{sol}} l,$$

where "sol" represents the summation over all soluble phases, α represents the absorption coefficient of each soluble phase, C represents the concentration of each soluble phase, and l is the thickness of the cuvette. Similarly, A_n is the absorbance due to the nth insoluble phase with $A_n = \alpha_n C_n l$.

This means that unless the absorption coefficients of each phase are known we cannot extract the absolute concentrations of each phase. Thus we work in terms of effective concentration as described above. In the limit where the absorption coefficients of all phases are equal, the effective concentration equals the real concentration.

For each of the solvents used, three samples were prepared by drop casting on holey carbon transmission electron microscopy (TEM) grids. Before sedimentation, and directly after sonication, a TEM grid of the dispersion in each solvent was prepared by drop casting. After the sedimentation, the sample was decanted to separate the sediment from the stable dispersion and TEM grids of both the sediment and the dispersion were prepared. TEM was performed using a Hitachi H-7000. High resolution TEM was carried out using a VG HB501 100 kV instrument. Field emission scanning electron microscopy was done using a Hitachi S-4300 on uncoated powder samples. The samples were also dispersed in isopropanol (IPA), and UV-visible-NIR spectra were taken using a Perkin-Elmer Lambda 9000 spectrometer, and a Kratos Axis HS and Mg $K\alpha$ x-ray source were used to measure their x-ray photoelectron spectra. Atomic force microscopy (AFM) measurements were also performed using a Nanoscope III on dispersions drop cast on highly ordered pyrolytic graphite (HOPG).

RESULTS AND DISCUSSION

Sedimentation studies

The dispersability of $Mo_6S_3I_6$ nanowires in various solvents—acetone, chloroform, *N*, *N*-dimethylformamide (DMF), dimethyl sulfoxide (DMSO), ethanol, isopropanol (IPA), 1-methyl-2-pyrrolidinone (NMP), and water—was measured to determine the best solvent for this material. The local effective concentration in the center of 0.1 g l^{-1} $Mo_6S_3I_6$ dispersions in these solvents was measured as a function of time for up to 750 h and these data are plotted in Fig. 1. For all solvents, the total effective concentration of the dispersions decreases with time, due to the sedimentation of insoluble material, until it reaches a constant value equal to the effective concentration of the stably dispersed material, when sedimentation is complete.

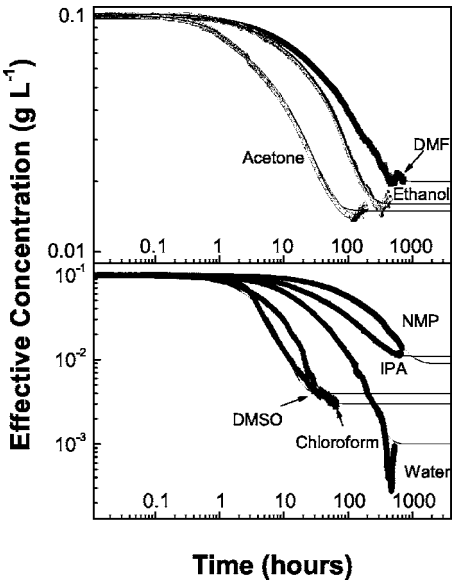

FIG. 1. Experimental sedimentation curves for 0.1 g l^{-1} dispersions of $Mo_6S_3I_6$ nanowire bundles in common solvents with biexponential fits shown as thin lines.

From Fig. 1, it can be seen that the $Mo_6S_3I_6$ behaves differently in each solvent with the rate of sedimentation and the final effective concentration varying. From these data, it is clear that DMF, acetone, and ethanol, shown in the upper panel of Fig. 1, have a significantly higher amount of stably dispersed material than those in the lower panel of Fig. 1.

From sedimentation theory, it is predicted that the concentration of any insoluble phase should decay exponentially with time. To test this, each sedimentation data set was fitted to Eq. (6). For all solvents, the best fit was found to be a biexponential decay with a constant component (except DMSO, which was best fitted by a single exponential). This implies that there are two insoluble components and one stably dispersed component in the $Mo_6S_3I_6$ material. These fits are shown in Fig. 1 as solid lines. From the fit, we can extract five parameters, the effective concentrations of each phase and the time constants: $C_{\text{eff},0}$, $C_{\text{eff},1}$, $C_{\text{eff},2}$, τ_1, τ_2, for each solvent as listed in Table I. As $C_{\text{eff},0}$, represents the stably dispersed material, these data indicate that the best solvents for the $Mo_6S_3I_6$ nanowires are DMF with $C_{\text{eff},0}/C_{\text{total}}$ of 20%, followed by acetone and ethanol with $C_{\text{eff},0}/C_{\text{total}}$ of 16% and 15%, respectively. NMP and IPA have a reasonable amount of material stably dispersed also, but water, DMSO, and chloroform all have $C_{\text{eff},0}/C_{\text{total}}$ less than 4% making them poor solvents.

It should be pointed out that the $C_{\text{eff},1}$ and $C_{\text{eff},2}$ values represent the effective concentrations of phases 1 and 2 in each solvent. However, like $C_{\text{eff},0}$, these quantities should only be taken as guidelines to the amount of each phase present. As discussed previously they are effective quantities and cannot be translated into real concentrations unless the absorption coefficients of the individual phases are known.

TEM grids were prepared from the dispersions in each solvent immediately after sonication (before sedimentation) and immediately after sedimentation had completed. In addition, a TEM grid was also prepared with the sediment after

Downloaded 01 Jul 2010 to 134.226.1.229. Redistribution subject to AIP license or copyright; see http://jap.aip.org/jap/copyright.jsp

TABLE I. Fit parameters from biexponential fits to the sedimentation data shown in Fig. 1 are shown in columns 1–5. In columns 6 and 7 the presence or absence of nanowires and impurities in each dispersion after sedimentation is indicated. NB the parameters given in columns 1, 2 and 4 are quoted to have zero error. This is not strictly true. The errors as calculated by the graphing software (Origin 7.5) were of order 10^{-4} to 10^{-5}. As such we have approximated them to zero in the table.

	$C_{\text{eff},0}/C_{\text{total}}$	$C_{\text{eff},1}/C_{\text{total}}$	τ_1 (h)	$C_{\text{eff},2}/C_{\text{total}}$	τ_2 (h)	NWs	Imps
DMF	0.2±0	0.34±0	13.6±0.04	0.46±0	122.1±0.15	Y	N
Ethanol	0.16±0	0.27±0	5.3±0.02	0.6±0	59.9±0.05	Y	Y
Acetone	0.15±0	0.39±0	2.1±0.02	0.48±0	18.7±0.03	Y	N
NMP	0.09±0	0.29±0	41.5±0.06	0.63±0	287.7±0.28	Y	Y
IPA	0.11±0	0.41±0	17.8±0.02	0.47±0	122.2±0.07	Y	N
Chloroform	0.03±0	0.18±0	1.8±0.03	0.8±0	9.0±0.02	Y	N
DMSO	0.04±0	0.99±0	4.3±0.02	···	···	N	Y
Water	0.01±0	0.63±0	14.2±0.02	0.36±0	84.9±0.11	N	N

sedimentation. Examples of these TEM images, taken for the best solvent, DMF, are shown in Fig. 2. The stably dispersed material, remaining after sedimentation, mainly consists of smaller diameter nanowire bundles, as shown in Fig. 2(a). Shown in Fig. 2(b) is a high resolution image of one of these bundles showing the individual nanowires. Before sedimentation, the dispersion contains large diameter bundles and pseudospherical impurities, as shown in Fig. 2(c). In contrast, the dispersions after sedimentation were free of impurity material as will be discussed below. The sediment consisted of very large diameter bundles and impurity material, as shown in Fig. 2(d). The dimensions of approximately 100 nanowire bundles in each of the best solvents (DMF, ethanol, acetone, and NMP) before and after sedimentation were measured and the averages are listed in Table II. This clearly shows that the material that remains dispersed after sedimentation consists of smaller diameter bundles relative to the original dispersion.

The as-produced $Mo_6S_3I_6$ material is in the form of needles with diameters ranging from 50 to 1000 nm, and up to 5 mm in length.[5] After sonication, pseudospherical impurities (similar to those seen in $Mo_6S_{4.5}I_{4.5}$)[8] and a large number of nanowire bundles were observed in all the solvents. The nanowire bundle diameters ranged from 56±55 to 133±360 nm and lengths from 0.9±1.2 to 1.2±1.6 μm in the best solvents, demonstrating the effectiveness of the sonication in breaking up the large bundles in the synthesized material. After sedimentation, the dimensions of the dispersed bundles had decreased to diameters of between 12±14 and 39±19 nm, and lengths of between 0.4±0.3 and 0.9±0.7 μm. This indicates that the larger diameter bundles have sedimented out leaving only the smaller bundles. The nanowire bundles in DMF, which was shown to be the best solvent, had the smallest average diameters at 12±14 nm, in agreement with this observation. The presence, or absence, of nanowires and impurities in the dispersions after sedimentation was noted for each solvent. The results are shown in the right-hand columns of Table I, labeled "NWs" for nanowires and "Imps" for impurities. "Y" in the relevant column indicates the presence of nanowires/impurities, and "N" indicates none are present. These results show that sedimentation of the $Mo_6S_3I_6$ nanowires in DMF is effective at purifying the material. Acetone retains slightly less nanowires making it a second possibility, whereas the rest of the solvents tested retain measurable amounts of impurities, or do not retain enough nanowires to make them a practical choice for purification.

DMSO behaved differently from all the other solvents. The best fit to the DMSO data was a single exponential, consistent with one sedimenting phase, whereas two distinct sedimenting phases were identified in all other solvents. No nanowires were observed in TEMs of the DMSO dispersion after sedimentation, unlike the other solvents which all contained significant amounts. DMSO appears unable to suspend either the impurities or the nanowires for longer than 36 h. Previously, it was shown that DMSO and chloroform were among the best solvents for dispersing $Mo_6S_{4.5}I_{4.5}$

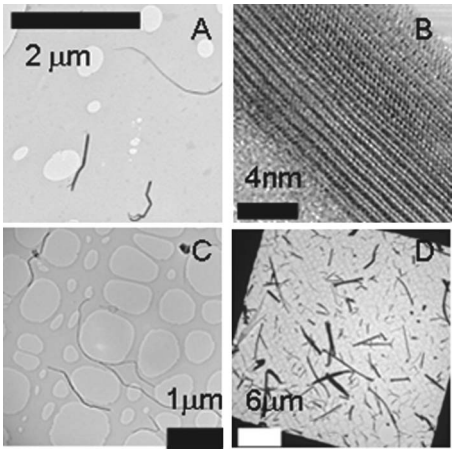

FIG. 2. Transmission electron microscopy images of the $Mo_6S_3I_6$ nanowire dispersion in DMF immediately after sonication (a), HRTEM image of a dispersed bundle (b), the dispersion after sedimentation (c), and the sediment after sedimentation (d).

TABLE II. Average lengths and diameters of $Mo_6S_3I_6$ nanowire bundles, as measured from TEMs, for the best solvents before and after sedimentation. These measurements are used in the plots in Fig. 4.

	d_{before} (nm)	L_{before} (μm)	d_{after} (nm)	L_{after} (μm)
DMF	60±66	0.9±1.2	12±14	0.6±0.4
Ethanol	133±360	1.2±1.3	33±22	0.7±0.5
Acetone	67±102	1.2±1.6	39±19	0.9±0.7
NMP	56±55	1.0±0.9	19±17	0.4±0.3

Downloaded 01 Jul 2010 to 134.226.1.229. Redistribution subject to AIP license or copyright; see http://jap.aip.org/jap/copyright.jsp

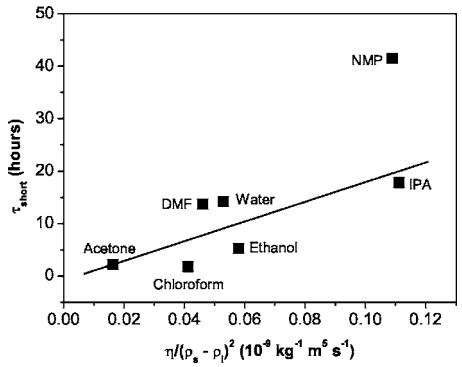

FIG. 3. τ_{short} for all solvents (except DMSO) plotted against parameters from Eq. (4).

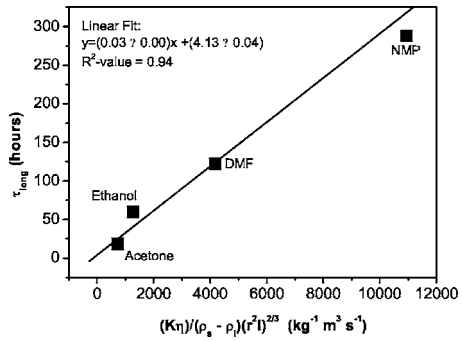

FIG. 4. τ_{long} for the best solvents plotted against the parameters for cylindrical particles as in Eq. (5), demonstrating agreement with sedimentation theory. The linear fit parameters to the data are included in the inset.

nanowires,[8] but these are amongst the worst solvents for dispersing the $Mo_6S_3I_6$ nanowires. Similarly, ethanol and acetone, which do not disperse $Mo_6S_{4.5}I_{4.5}$, do disperse $Mo_6S_3I_6$. Although, DMF disperses both nanowire stoichiometries, the results for these other solvents indicate dramatically different dispersion properties of the MoSI nanowire stoichiometries. This clearly indicates the fact that the surface arrangement of atoms, i.e., those that interact with the solvent, must be different for $Mo_6S_{4.5}I_{4.5}$ and $Mo_6S_3I_6$.[22]

For each solvent, except DMSO, the time constants for the two sedimenting phases, τ_1 and τ_2, were calculated from the fits to the experimental data using Eq. (6). For each solvent (except DMSO) the two time constants have been characterized as short and long, the short time constant representing the material that sediments first. As discussed above, the impurity material tends to sediment out of most solvents to a reasonable degree. This suggests that the short time constant represents the pseudospherical impurity material. This has been confirmed for $Mo_6S_{4.5}I_{4.5}$ nanowires.[8,10] Thus the short time constant should be described by Eq. (4) which is appropriate to spherical objects. Equation (4) predicts that the time constant should scale with $\eta/(\rho_s - \rho_l)$. In Fig. 3, the shorter time constant, which we will refer to as τ_{short}, is plotted against $\eta/(\rho_s - \rho_l)$ for all solvents (except DMSO). If we ignore NMP, the trend is approximately linear as would be predicted from Eq. (4). The deviations from linearity are to be expected as Eq. (4) shows that τ_{short} also depends on the diameter of the sedimenting particles. These particles are thought to be aggregates of smaller impurity particles. Thus the degree to which they break up on sonication and hence the dimensions of the sedimenting particles may vary between solvents.

In analogy with previous work on $Mo_6S_{4.5}I_{4.5}$ the longer time constant, τ_{long}, is expected to relate to nanowire bundles that are unstable in the solvents studied. Due to their high aspect ratio and small radius, these cylindrical objects tend to sediment slowly as predicted by Eq. (5). In addition, cylinders have a higher drag coefficient relative to spheres further slowing sedimentation.[23] The nature of the second sedimenting phase will be confirmed by SEM in the next section.

According to Eq. (5), τ_{long} depends on the solvent viscosity η, the density difference between solvent and sedimenting object $(\rho_s - \rho_l)$, and the dimensions of the sedimenting object r and l, both directly and indirectly through the drag coefficient K. In Fig. 4, τ_{long} is plotted for the four best solvents, as a function of $K\eta/(\rho_s - \rho_l)(r^2 l)^{2/3}$. The average lengths and average diameters used are approximated with those measured before sedimentation, as quoted in Table II. The drag coefficient was calculated using these bundle dimensions.[23] This results in an excellent linear fit encompassing all four solvents. We can use this fit to calculate $(\beta - p_f)$ to be ~1900 Pa. In the cuvette used for these experiments, the fluid pressure is always very close to atmospheric pressure. This means that β is within 2% of atmospheric pressure. The authors have been unable to find any other numerical value for β quoted in the literature for any system.

Purification by sedimentation and analysis

From the calculated time constants for the sedimenting phases in DMF, τ_1 and τ_2 (τ_{short} and τ_{long}), it can be shown that phases 1 and 2 will have almost completely sedimented from solution after approximately 70 and 600 h, respectively. In Fig. 5, this is illustrated by showing the experimental data with the fit and the theoretical sedimentation curves for each phase generated from the fit. Therefore, the two sediments and the solute can be separated by carefully decanting after 70 h to give a sediment of mainly phase 1, and after 600 h to give a sediment of mainly phase 2. The remaining solvent will contain the solute. It should be pointed that perfect separation can never be achieved in this manner, only significant enrichment of a given phase.

A 1 g l^{-1} dispersion of the $Mo_6S_3I_6$ material in DMF was prepared by sonication and was allowed to sediment for

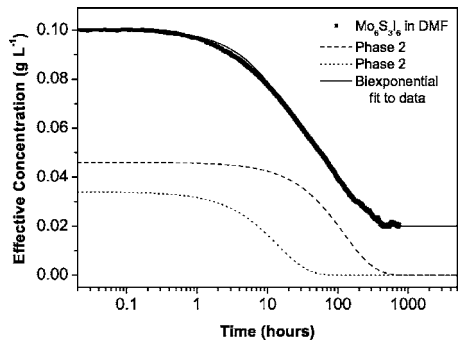

FIG. 5. Normalized effective concentration of $Mo_6S_3I_6$ in DMF with biexponential fit (solid line), and decay curves as calculated for sedimenting phase 1 (dotted line) and sedimenting phase 2 (dashed line).

Downloaded 01 Jul 2010 to 134.226.1.229. Redistribution subject to AIP license or copyright; see http://jap.aip.org/jap/copyright.jsp

70 h before being decanted. The dispersion was then sonicated again and allowed to sediment for 600 h before being decanted a second time. The remaining dispersion was dried in a vacuum oven with the two sediments and these three dried powders were weighed. Initially, 24.7 mg of washed $Mo_6S_3I_6$ material was dispersed in DMF. The masses of sediment 1, sediment 2, and the solute recovered were 19.7 mg (~87%), 1.5 mg (~7%), and 1.4 mg (~6%), respectively, with 2.1 mg unrecoverable. It must be emphasized that these values are proportional to the *true* concentrations of the three phases should not scale with the fit values for the *effective* concentrations, $C_{\text{eff},1}$, $C_{\text{eff},2}$, and $C_{\text{eff},0}$ measured for the DMF dispersions.

Therefore, after 600 h 6% of the $Mo_6S_3I_6$ was still dispersed in DMF, at a concentration of approximately 0.06 g l^{-1}. It is not clear whether this represents a solubility limit or perhaps the fact that the fraction of dispersible material in the washed powder was low. Nevertheless it shows that it is possible to produce stable dispersions of $Mo_6S_3I_6$ with concentrations as high as 0.06 g l^{-1}. This compares reasonably well with achieved concentrations of 0.34 g l^{-1} for $Mo_6S_{4.5}I_{4.5}$ in isopropanol[10] or indeed of 0.02 g l^{-1} for single walled nanotubes in NMP.[20]

UV-visible-NIR spectroscopy

Each of the three recovered powders, sediment 1, sediment 2, and the solute were redispersed in IPA (C ~1.5 mg/ml). For comparison purposes, the $Mo_6S_3I_6$ soot was also dispersed in IPA. It should be pointed out that each phase was generally insoluble in IPA. However, measurements could be made before any significant sedimentation had occurred. UV-visible-NIR spectroscopy in the range from 0.5 to approximately 4 eV was performed on these solutions and the recorded spectra, as well as a reference IPA spectrum, are shown in Fig. 6. In all four spectra, and as observed in similar spectra for $Mo_6S_{4.5}I_{4.5}$,[8] there are broad peaks visible at approximately 2.7 and 1.75 eV in the visible region. The main differences are observed in the near-IR region (~0.6–0.8 eV) and this region of the spectra is shown in greater detail in Figs. 6(a)–6(d). In the range from approximately 0.7 to 0.75 eV, there is much noise due to the subtraction of the IPA peaks from the individual spectra so no peaks are visible. In sediment 2 and in the solute a distinct peak is observed at 0.64 eV with a smaller shoulder at 0.66 eV. This demonstrates the similarity between these two phases, which both mainly contain $Mo_6S_3I_6$ nanowires, as observed in the TEM and SEM images. Such a feature has also been observed for $Mo_6S_{4.5}I_{4.5}$ nanowires.[8] The position of this peak agrees well with predictions for the MoSI band gap[12] suggesting that it may represent a transition involving the van Hove singularity associated with the band edge. All these features are visible in the washed $Mo_6S_3I_6$ sample, which should be a combination of these three phases, as was expected, although the peak at 0.64 eV is quite weak due to the high intensity of the near infrared peaks in sediment 1. At 0.64 eV in the sediment 1 spectrum, all that is visible is noise due to the IPA peaks present in this region.

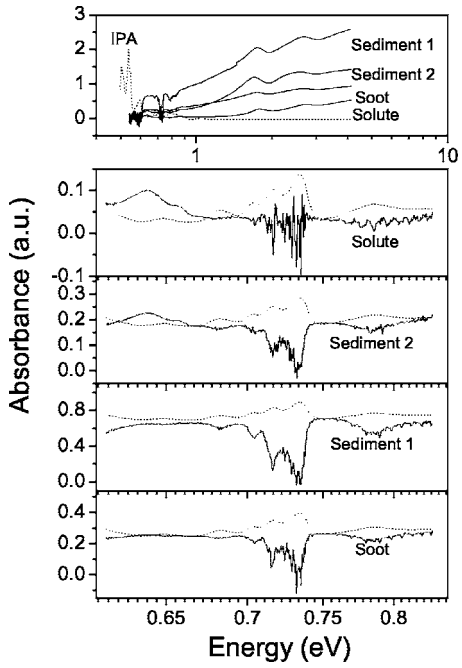

FIG. 6. UV-visible-IR absorption spectra of the raw $Mo_6S_3I_6$ powder, the solute and the two sediments dispersed in IPA are shown in the top graph. The near-IR region for each material is shown in greater detail in the spectra below. In all spectra, the IPA spectrum is shown as a dotted line.

X-ray photoelectron spectroscopy

X-ray photoelectron spectroscopy was also performed on the three phases, and on the as-produced (unwashed) and washed $Mo_6S_3I_6$ raw material, dispersed in IPA to analyze the differences in the elemental components. The dispersions were deposited on silicon dioxide substrates and the spectra were analyzed, ignoring the SiO_2 peaks, to determine the stoichiometries of the different samples. The molybdenum, iodine, sulfur, and oxygen spectra for the solute material are shown in Fig. 7, and similar spectra were obtained and analyzed for the other samples. The calculated stoichiometry for the as-produced material was $Mo_6S_{4.3}I_{11.8}$. However, after washing with acetone, the stoichiometry became $Mo_6S_{4.5}I_{8.6}$ showing the excess iodine content has been substantially reduced. For the two sediments, the calculated stoichiometries were $Mo_6S_{11}I_{0.8}$ for sediment 1 and $Mo_6S_{3.5}I_{7.9}$ for sediment 2. The stoichiometry of sediment 1 suggests it is mainly MoS_2 with traces of iodine present, which have been reported in the as-produced material[5] and in the $Mo_6S_{4.5}I_{4.5}$ material.[8] In addition, we cannot rule out the presence of some nanowires. Sediment 2 is consistent with being mainly $Mo_6S_3I_6$ nanowires, but it is clear that there are still traces of MoS_2 and excess iodine present, as the determined stoichiometry has higher proportions of sulfur and iodine than the $Mo_6S_3I_6$ stoichiometry. This concurs with the sedimentation theory that the pseudospherical MoS_2 impurities would sediment faster than the nanowires, hence sediment 1 is mainly MoS_2 and sediment 2 is mainly $Mo_6S_3I_6$ nanowires. It is not clear why the nanowires contained in sediment 2 are insoluble while the nanowires contained in the solute can be dispersed. There are two possibilities. It may be that the solubility limit of these nanowires in each solvent governs the amount of stable nanowires. Alternatively, it is possible that

Downloaded 01 Jul 2010 to 134.226.1.229. Redistribution subject to AIP license or copyright; see http://jap.aip.org/jap/copyright.jsp

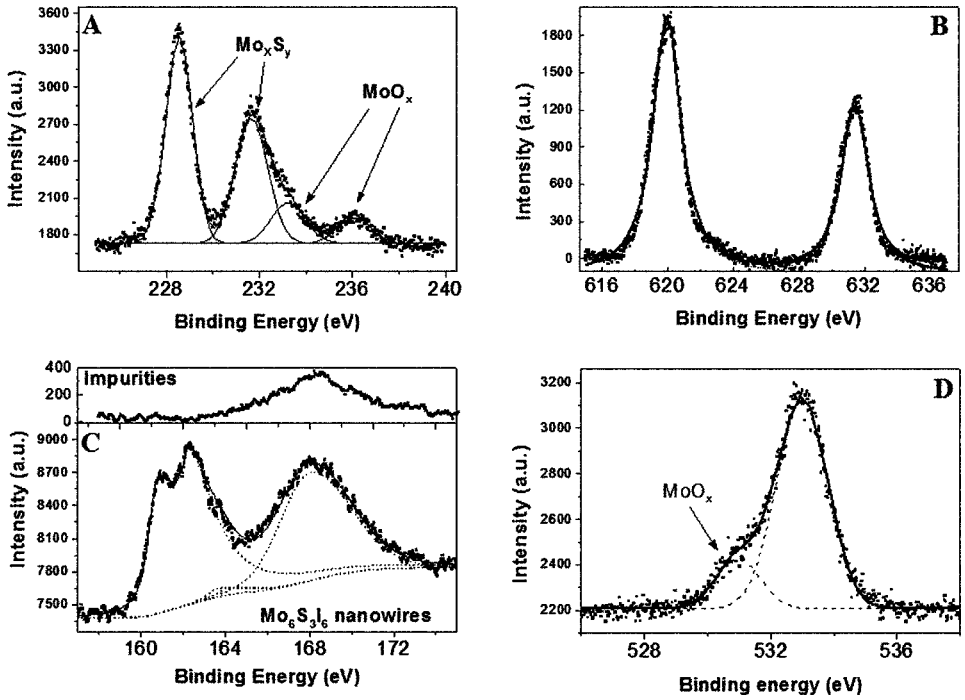

FIG. 7. X-ray photoelectron spectra of the stably dispersed material from the DMF separation. Molybdenum 3*d* spectrum is shown in Fig. 6(a), iodine 3*d* spectrum in Fig. 6(b), sulfur 2*p* in Fig. 6(c) (and the upper inset is the sulfur 2*p* spectrum of phase 1), and Fig. 6(d) is the oxygen 1*s* spectrum. In all the spectra, the experimental data are points, the experimental fits are shown as solid lines, and the deconvoluted peaks are shown as dotted lines.

the dispersed nanowires are chemically different to the ones that sediment. It is not clear that this difference is one of stoichiometry or of surface atomic arrangement. Further studies are required to answer these questions.

A more detailed analysis was performed on the solute XPS data, shown in Fig. 7, during which two pairs of doublets associated with MoS_x (228.6 and 231.7 eV) and MoO_y (233.35 and 236 eV) were identified. These doublets are both due to molybdenum $3d_{5/2}$ and $3d_{3/2}$ spin-orbit splitting. From the analysis of the oxygen spectrum, and after disregarding the peak due to the SiO_2 substrate (533 eV), a peak due to a MoO_y compound was observed leading to the stoichiometry of the compound being determined as $MoO_{3.7}$. This compound was also identified as being formed at between 300 and 500 °C during the thermogravimetric analysis (TGA) of the raw material, as previously reported.[5] This compound can be formed by the "roasting" of MoS_2 at atmospheric pressure at temperatures around 315 °C.[24] It is likely that this compound was formed as a by-product during the material synthesis or during sonication. In the sulfur spectrum, several contributions were distinguished, with one peak relating to sulfur oxides (168.2 eV) [e.g., sulfates (SO_4^{2-}), sulfides (SO_3^{2-}), sulfur dioxide (SO_2), etc.], a pair of $2p_{5/2}$ and $2p_{3/2}$ spin-orbit split peaks relating to MoS_x species (160.9 and 162.3 eV), and a second pair of $2p_{5/2}$ and $2p_{3/2}$ spin-orbit split peaks relating to S–I species (163.4 and 164.6 eV). The sulfur oxide peak corresponds with a peak observed in sediment 1 (inset) showing it was impossible to remove absolutely all impurities after separation. This is also true for the iodine, as the full width at half maximum of the iodine peaks shows that multiple species of iodine are present in the solute, indicating not all the excess iodine was removed. Disregarding the SO_x peak at 168.2 eV, the stoichiometry of the solute was calculated to be $Mo_6S_{3.1}I_{7.4}$, which is very close to the predicted stoichiometry of $Mo_6S_3I_6$. There are still excess iodine and various SO_x compounds present as they are soluble in the DMF, but there are only traces of any other impurities. It is probable that the iodine and SO_x species could be removed by further washing after the separation with an alternative solvent. The XPS results show that, besides the iodine and SO_x, there are only trace impurities present in the solute and the purity has been greatly improved from the raw material whose stoichiometry is $Mo_6S_{4.3}I_{11.8}$.

SEM

To further analyze the different phases SEM was performed on dried powders of phases 1 and 2, the solute, and the washed raw material. Representative SEM images of each of these are shown in Fig. 8, with the images on the right are all at approximately the same magnification to allow direct comparison. The initial material contains large nanowire bundles and large pseudospherical impurities that are also seen in sediment 1. Sediment 2 contains smaller nanowire bundles and few, small impurities. The solute only contains very small bundles, relative to the sediments, and almost no impurities.

The XPS and the SEM have shown that the solute contains purified $Mo_6S_3I_6$ nanowires, and that sedimentation is an effective method of purifying this material as the impurities and larger diameter nanowire bundles sediment out of solution in a shorter time than the smaller diameter nanowire bundles. Using this technique, stable dispersions of purified $Mo_6S_3I_6$ nanowires in DMF can be produced.

Downloaded 01 Jul 2010 to 134.226.1.229. Redistribution subject to AIP license or copyright; see http://jap.aip.org/jap/copyright.jsp

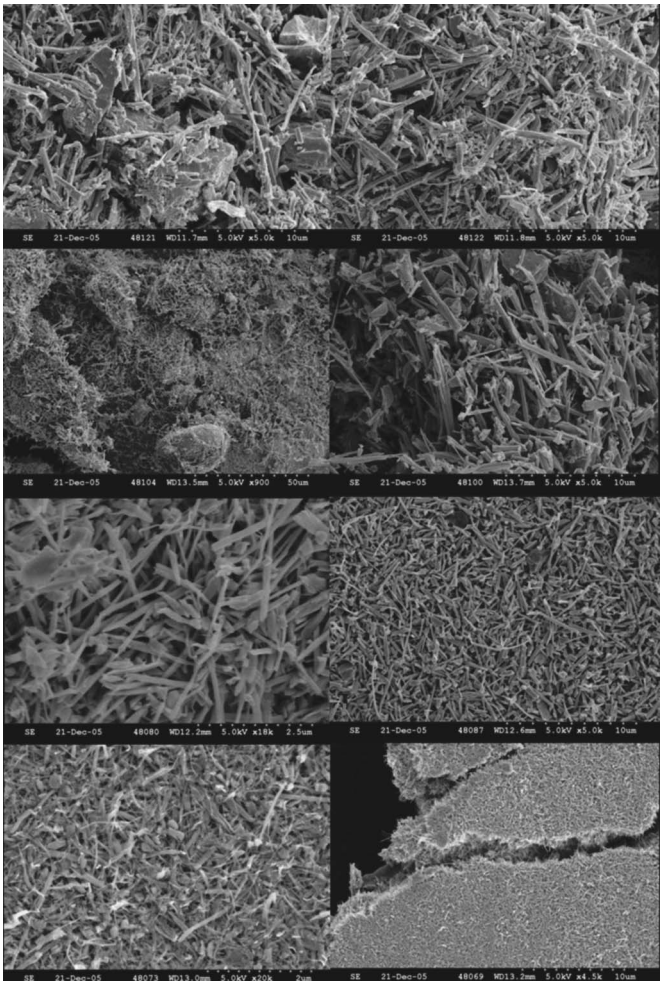

FIG. 8. Scanning electron microscopy images of washed as-produced $Mo_6S_3I_6$ material (first row), sediment 1 (second row), sediment 2 (third row), and the solute (fourth row).

AFM measurements

Although the dimensions of the $Mo_6S_3I_6$ nanowires have been measured using TEM, further measurements were performed using AFM, as the resolution of the TEM was not sufficient to image individual nanowires. The bundle diameters for a range of concentrations of the purified $Mo_6S_3I_6$ solute, from 0.1 to 0.001 g l^{-1}, have been measured and the results are shown as histograms in Fig. 9. These histograms show that as the concentration decreases, the diameter distribution narrows and is downshifted, until at 0.001 g l^{-1} the diameter of the majority of nanowires are approximately 2 nm, corresponding to a bundle of two to four nanowires. This is clearly shown in Fig. 10(a), where the mean diameter of the nanowire bundles, as calculated from the distributions shown in Fig. 9, is observed to decrease with decreasing concentration. From the AFM measurements, we can calculate the number fraction of individual nanowires, as this is the number of individual nanowires (bundles with diameter less than ~1.2 nm) divided by the total number of nanowire bundles measured for each sample. This is plotted against concentration in Fig. 10(b) and shows that the number of individual nanowires present is proportional to the concentration. These results show that individual $Mo_6S_3I_6$ nanowires are present at all concentrations, as can be seen in the histograms in Fig. 9, and solutions of mainly individual nanowires are achievable by dilution.

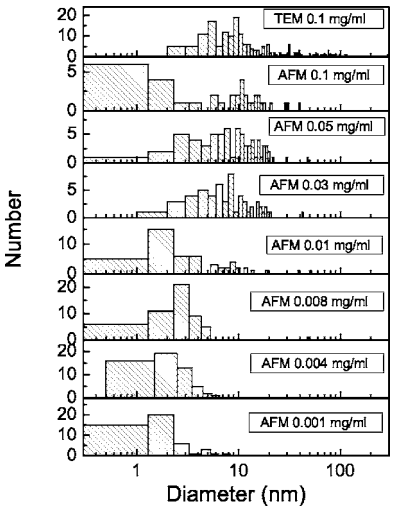

FIG. 9. Histograms of the bundle diameters for $Mo_6S_3I_6$ nanowires dispersed in isopropanol at a range of concentrations from 0.1 to 0.001 mg/ml. Diameters have been measured from AFM images taken immediately after sonication. Decreases in concentration are accompanied by a downshift of the diameter distribution. For comparison purposes a diameter distribution representing the 0.1 mg/ml sample but measured by TEM is shown in the top panel.

Aligned $Mo_6S_3I_6$ nanowires

SEM was performed on dried powders of the different phases. In Fig. 11, four SEM images of a particle of the solute phase that has dried with aligned nanowires is shown. In Fig. 11(a), the particle is visibly different from the others as it is brighter. In Fig. 11(b), the surface appears to be stratified layers, but at higher magnification, it can be seen that this is a surface of nanowires aligned preferentially in the direction indicated in Fig. 11(c). The mechanism causing this alignment is not known. As this material was subjected to extensive sonication and allowed to stand for 600 h, it is not

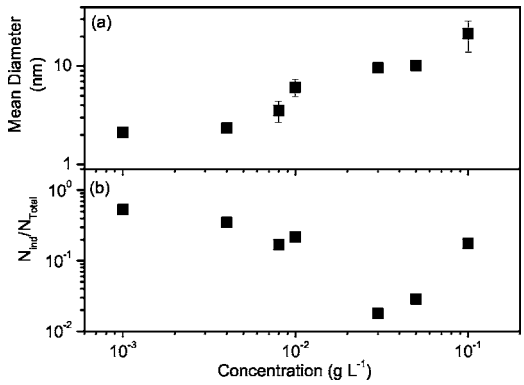

FIG. 10. (a) shows the mean diameter of nanowire bundles as a function of concentration as calculated from the diameter distributions in Fig. 9. The error bars represent the standard deviation. The mean bundle diameter decreases with decreasing concentration before saturating at approximately 2 nm. In (b), the number fraction of individual $Mo_6S_3I_6$ nanowires as a function of concentration as calculated from Fig. 9 is shown.

Downloaded 01 Jul 2010 to 134.226.1.229. Redistribution subject to AIP license or copyright; see http://jap.aip.org/jap/copyright.jsp

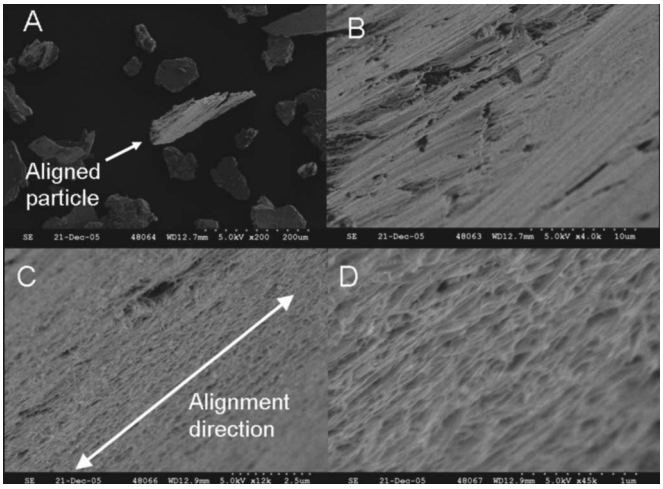

FIG. 11. Scanning electron microscopy images of aligned $Mo_6S_3I_6$ nanowires observed in the solute after drying.

possible for this to be a remnant of the raw material and must have been formed during drying of the solute material.

CONCLUSIONS

The local effective concentration of dispersions of washed $Mo_6S_3I_6$ raw material was measured as a function of time in several common solvents during the sedimentation of insoluble material. By fitting these data to the theory, it was calculated that for all solvents, except DMSO, two sedimenting phases and one stable phase were identified in the $Mo_6S_3I_6$ material (for DMSO, the best fit was one sedimenting and one stable phase). From the fit parameters and the TEM images DMF was determined to be the best solvent for the $Mo_6S_3I_6$ material, followed by acetone. These solvents stably disperse significantly larger amounts of the $Mo_6S_3I_6$ material than the other solvents and almost no impurities. Transmission electron microscopy was performed on these dispersions before sedimentation, after sedimentation and on the sediment after sedimentation. It was observed that the dispersions after sedimentation contained smaller diameter nanowire bundles than the dispersions before sedimentation. Stable dispersions of the nanowire material in DMF at concentrations of approximately 0.06 g l^{-1} were observed, making DMF an effective solvent and sedimentation an effective purification method.

The two sediment phases and the stably dispersed material were separated and analyzed using UV-visible-IR spectroscopy, SEM, and XPS. From the SEM it was observed that the washed raw $Mo_6S_3I_6$ material contained large diameter nanowire bundles and large amounts of impurities. Sediment 1 contained some nanowire bundles and large quantities of impurities. Sediment 2 contained smaller nanowire bundles and some impurities, and the soluble phase contained almost no impurities and very small nanowire bundles. This agrees very well with sedimentation theory predictions that high aspect ratio particles (nanowire bundles) will have a higher frictional coefficient than spherical particles (impurities). This would result in impurities sedimenting from solution faster than the nanowires, as is observed by the lack of impurities in sediment 2 and the soluble phase.

Although, there were no differences observed in the ultraviolet and visible regions of the UV-visible-IR spectra of the four samples, a peak was observed at 0.64 eV in the near-IR region for both the soluble phase and sediment 2, that was not observed in either sediment 1 or the washed raw material. As observed from SEM, the soluble phase and sediment 2 are mainly small diameter nanowire bundles and are significantly different from the other two samples. This peak can therefore be associated with the purified nanowires, which further supports the predictions of sedimentation theory.

From the XPS of the different samples, the stoichiometries were calculated. The stoichiometry calculated for the three separated phases were $Mo_6S_{11}I_{0.8}$ for sediment 1, $Mo_6S_{3.5}I_{7.9}$ for sediment 2, and $Mo_6S_{3.1}I_{7.4}$ for the soluble phase. These results confirm the previous findings, showing quite clearly that the first sediment is mainly the impurity material MoS_2, and the second sediment containing mainly $Mo_6S_3I_6$ nanowires and some traces of impurities. Although some traces of DMF soluble impurities, such as molybdenum trioxide and some sulfur oxides were identified, the soluble phase stoichiometry is consistent with being almost completely $Mo_6S_3I_6$ nanowires and approximately 12% by mass excess iodine. These impurities and the iodine could be removed by washing with an alternative solvent.

These results demonstrate the ease with which the $Mo_6S_3I_6$ nanowires can be stably dispersed in certain solvents and at relatively high concentrations. This, combined with their monodisperse electronic structure and high Young's modulus, makes them more attractive for applications than carbon nanotubes. The simple, one-step synthesis of these nanowires, which can easily be scaled up, also gives them a significant advantage. These properties of the $Mo_6S_3I_6$ nanowires suggest a wide range of future applications for this material.

DM and WJB would like to acknowledge EU Specific Targeted Research Project DESYGN-IT (No. NMP4-CT-2004-505626) for support.

[1] A. B. Greytak, L. J. Lauhon, M. S. Gudiksen, and C. M. Lieber, Appl. Phys. Lett. **84**, 4176 (2004).
[2] Y. Xia, P. Yang, Y. Sun, Y. Wu, B. Mayers, B. Gates, Y. Yin, F. Kim, and H. Yan, Adv. Mater. (Weinheim, Ger.) **15**, 353 (2003).
[3] J. N. Coleman, U. Khan, W. J. Blau, and Y. K. Gun'ko, Carbon **44**, 1624 (2006).
[4] R. H. Baughman, A. A. Zakhidov, and W. A. de Heer, Science **297**, 787 (2002).
[5] D. Vrbanic *et al.*, Nanotechnology **15**, 635 (2004).
[6] Mo6 d.o.o., http://www.mo6.com (2006).
[7] PCT/EP2004/001870 (2004).
[8] V. Nicolosi *et al.*, J. Phys. Chem. B **109**, 7124 (2005).
[9] V. Nicolosi, D. Vengust, D. Mihailovic, W. J. Blau, and J. N. Coleman, Chem. Phys. Lett. **425**, 89 (2006).
[10] V. Nicolosi, D. Vrbanic, A. Mrzel, J. McCauley, S. O'Flaherty, D. Mihailovic, W. J. Blau, and J. N. Coleman, Chem. Phys. Lett. **401**, 13 (2005).
[11] M. Remskar, A. Mrzel, Z. Skraba, A. Jesih, M. Ceh, J. Demsar, P. Stadelmann, F. Levy, and D. Mihailovic, Science **292**, 479 (2001).
[12] A. Meden, A. Kodre, J. Padeznik Gomilsek, I. Arcon, I. Vilfan, D. Vrbanic, A. Mrzel, and D. Mihailovic, Nanotechnology **16**, 1578 (2005).

Downloaded 01 Jul 2010 to 134.226.1.229. Redistribution subject to AIP license or copyright; see http://jap.aip.org/jap/copyright.jsp

[13]B. Bercic, U. Pirnat, P. Kusar, D. Dvorsek, D. Mihailovic, D. Vengust, and B. Podobnik, Appl. Phys. Lett. **88**, 173103 (2006).
[14]A. Hassanien, M. Tokumoto, A. Mrzel, D. Mihailovic, and H. Kataura, Physica E (Amsterdam) **29**, 684 (2005).
[15]L. Joly-Pottuz, F. Dassenoy, J. M. Martin, D. Vrbanic, A. Mrzel, D. Mihailovic, W. Vogel, and G. Montagnac, Tribol. Lett. **18**, 385 (2005).
[16]M. Zumer, B. Zajec, N. Vincenc, Z. Bojan, R. Maja, P. Mihaela, V. Damjan, M. Ales, and M. Dragan, Nanotechnology **16**, 1619 (2005).
[17]R. Murphy *et al.*, Scr. Mater. **54**, 417 (2006).
[18]C. A. Furtado, U. J. Kim, H. R. Gutierrez, L. Pan, E. C. Dickey, and P. C. Eklund, J. Am. Chem. Soc. **126**, 6095 (2004).
[19]B. J. Landi, H. J. Ruf, J. J. Worman, and R. P. Raffaelle, J. Phys. Chem. B **108**, 17089 (2004).
[20]S. Giordani, S. D. Bergin, V. Nicolosi, S. Lebedkin, M. M. Kappes, W. J. Blau, and J. N. Coleman, J. Phys. Chem. B **110**, 15708 (2006).
[21]M. Tory, *Sedimentation of Small Particles in a Viscous Fluid* (Computational Mechanics, Southampton, 1996).
[22]V. Nicolosi *et al.*, Adv. Mater. (Weinheim, Ger.) (to be published).
[23]V. A. Davis *et al.*, Macromolecules **37**, 154 (2004).
[24]G. Leichtfried, *Ullmans Encycopedia of Industrial Chemistry*, 5th ed. (Wiley, New York, 1990), Vol. A16.

Downloaded 01 Jul 2010 to 134.226.1.229. Redistribution subject to AIP license or copyright; see http://jap.aip.org/jap/copyright.jsp